frontiers in Immunology

ORIGINAL RESEARCH
published: 21 May 2021
doi: 10.3389/fimmu.2021.687242

Plasma Membrane Calcium ATPase Regulates Stoichiometry of CD4$^+$ T-Cell Compartments

*Maylin Merino-Wong, Barbara A. Niemeyer and Dalia Alansary**

Molecular Biophysics, Saarland University, Homburg, Germany

Immune responses involve mobilization of T cells within naïve and memory compartments. Tightly regulated Ca^{2+} levels are essential for balanced immune outcomes. How Ca^{2+} contributes to regulating compartment stoichiometry is unknown. Here, we show that plasma membrane Ca^{2+} ATPase 4 (PMCA4) is differentially expressed in human CD4$^+$ T compartments yielding distinct store operated Ca^{2+} entry (SOCE) profiles. Modulation of PMCA4 yielded a more prominent increase of SOCE in memory than in naïve CD4$^+$ T cell. Interestingly, downregulation of PMCA4 reduced the effector compartment fraction and led to accumulation of cells in the naïve compartment. *In silico* analysis and chromatin immunoprecipitation point towards Ying Yang 1 (YY1) as a transcription factor regulating PMCA4 expression. Analyses of PMCA and YY1 expression patterns following activation and of PMCA promoter activity following downregulation of YY1 highlight repressive role of YY1 on PMCA expression. Our findings show that PMCA4 adapts Ca^{2+} levels to cellular requirements during effector and quiescent phases and thereby represent a potential target to intervene with the outcome of the immune response.

Keywords: Plasma Membrane Calcium ATPase, Yin Yang 1, CD4$^+$ compartments, calcium signaling, stoichiometry

OPEN ACCESS

Edited by:
Andrew D. Wells,
Children's Hospital of Philadelphia, United States

Reviewed by:
Tomasz Boczek,
Boston Children's Hospital and Harvard Medical School, United States
Kai Yang,
Indiana University School of Medicine-Lafayette, United States

****Correspondence:***
Dalia Alansary
dalia.alansary@uks.eu

Specialty section:
This article was submitted to T Cell Biology, a section of the journal Frontiers in Immunology

Received: *29 March 2021*
Accepted: *04 May 2021*
Published: *21 May 2021*

Citation:
Merino-Wong M, Niemeyer BA and Alansary D (2021) Plasma Membrane Calcium ATPase Regulates Stoichiometry of CD4$^+$ T-Cell Compartments. Front. Immunol. 12:687242. doi: 10.3389/fimmu.2021.687242

INTRODUCTION

The spatiotemporal characteristics of Ca^{2+} signals in T cells tightly control the outcome of an immune response as well as the fate of the immune cells involved. A local or global rise of intracellular $[Ca^{2+}]_i$ is achieved by activation of Ca^{2+} channels or by mobilization from intracellular stores. Once the Ca^{2+} signal is conducted, extrusion pumps restore the resting concentration. Alternatively, resting concentration is restored by Ca^{2+} uptake into intracellular stores: mitochondria or endoplasmic reticulum (ER).

Plasma membrane Ca^{2+} ATPase (PMCA) is the major extrusion pump playing a pivotal role in the regulation of Ca^{2+} dynamics during activation of T cells (1–4) in co-operation with sodium calcium exchanger (NCX) (5) and the sarco-endoplasmic reticulum Ca^{2+} ATPase (SERCA) (6). In addition to its global role, PMCA is able to generate local gradient in its vicinity thereby influencing Ca^{2+} dependent interaction partners (7). Furthermore, PMCA interacts with the inhibitory domain of CD147 in a Ca^{2+} independent manner which is necessary for CD147-mediated inhibition of IL-2 production (8). PMCA is a type-P ATPase of the class PIIB (9). In mammals PMCA contains a C-terminal auto-inhibitory domain, by which the inhibition is alleviated by binding to calmodulin or acidic phospholipids which can also bind to a basic domain in the first cytosolic loop [reviewed

in (10)]. There are four genes expressing PMCA (*ATP2B1–4*) with two possible splice sites resulting in a sum of about 30 variants belonging to four isoforms (11). All isoforms of PMCA have Ca^{2+} dependent activity with PMCA4b being the slowest isoform despite a higher affinity to Ca^{2+}/calmodulin than PMCA4a (12). The immunoglobulin proteins basigin and neuroplastin were identified as obligatory subunits of PMCA isoforms (13, 14). Co-assembly into a complex with either protein is necessary for stable PMCA surface localization in rat brain derived neurons (14), but also murine cells lacking neuroplastin showed reduced expression of PMCA (13).

The past four decades witnessed the development of models describing the differentiation of naïve T cells following antigen encounter into different compartments of effector and memory cells. These models are based on flow cytometric phenotypic analysis, and their outcome provides the basis for a nomenclature of subpopulations and describes function and persistence of populations arising during antigen encounter and clearance [for comprehensive reviews see (15–17)]. There are three main models describing memory cell generation. The first is based on epigenomic profiling and proposes linear development of naïve into stem central memory (TSCM) then CM, followed by effector memory (EM) and eventually effector (E) cells (15). The bifurcative model suggests that naïve cells asymmetrically divide to directly develop into E cells and in parallel an EM that gives rise to a CM lineage. The third model overlaps with the linear model with the effector cells retaining ability for self-renewal and hence the name of the model (18). Despite the intensive efforts, the mechanisms regulating naïve-to-memory cell transition are not entirely understood. One important aspect of this transition is the transcriptional reprogramming of the cells (19, 20). Through iterative interactions, transcription factors selectively combine genes to be expressed to define cytokine production and survival potential profiles characteristic of cell populations. Ca^{2+} dependence is a common feature of many of the transcription factors involved in T cell differentiation such as NFAT (21, 22), CREB (23) and the transcription repressor DREAM (24). The main pathway for Ca^{2+} influx in T cells is the store operated Ca^{2+} entry (SOCE) constituted by the channel forming ORAI proteins (25, 26) and the activator ER-resident Ca^{2+} sensor STIM proteins (27–29). While Ca^{2+} levels influence the activity of transcription factors, conversely, the expression of SOCE components (30) and also expression of proteins involved in Ca^{2+} homeostasis are subjected to transcriptional control (31). Transcriptional control of PMCA is, however, poorly understood and whether this control is altered during naïve-to-memory cell transition is yet to be explored. Therefore, we set out in the current study to investigate how PMCA alters Ca^{2+} signals in T cells to promote activation and differentiation; and to gain insight into mechanisms regulating PMCA expression during T cell activation.

MATERIALS AND METHODS

T-Cell Isolation and *In Vitro* Polarization

Blood samples were collected from healthy donors in the Institute of Clinical Hemostaseology and Transfusion Medicine, Saarland University, Homburg. The research was approved by the local ethical committee (83/15; FOR2289-TP6, Niemeyer/Alansary), and blood donors provided their written consent. Following thrombocyte apheresis, peripheral blood mononuclear cells (PBMCs) were isolated from leukocyte reduction chambers (LRS, Trima Accel®) according to (32, 33). Lymphocytes where enriched by overnight incubation of PBMCs to remove adherent monocyte and macrophages. On the next day $CD4^+$ cells were stained and naïve ($CD4^+CD127^{high}CD25^-CD45RO^-$) or memory ($CD4^+CD127^{high}CD25^-CD45RO^+$) cells were sorted using FACSAria III (BD). Isolated $CD4^+$ cells were seeded at density of 2×10^6 cells/ml in AIMV medium containing 10% FCS and 1% Pen/Strep and cultured for at least 24 h before conducting the experiments. Where indicated, naïve cells were polarized *in vitro* into Th1 or Treg according to (34). Alternatively, where indicated, total $CD4^+$ T cells were obtained from PBMC using negative isolation Kit (Miltenyi, #130-096-533) and automated cell isolation system (Mitenyi, AutoMACS).

Transfection

For downregulation of PMCA, 2×10^5 cells were seeded in 96-well plate in Accell siRNA Delivery Media (ADM, Horizon) supplemented with 10 ng/ml of recombinant IL-2 and transfected with 1 μM accel siRNA targeting ATP2B4 (Accell Human ATP2B4 siRNA-SMARTpool, E-006118-00-0005, Horizon) or non-silencing control RNA (Accell Non-targeting Pool, D-001910-10-05, Horizon) according to the manufacturer's instructions. Seventy-two hours later cells were harvested for mRNA or functional analysis.

Flow Cytometric Analysis

For flow cytometric analysis, cells were harvested, washed then stained with a viability dye (Zombie Aqua Fixable Viability Kit, Biolegend) followed by surface staining. Antibodies used for staining were supplied by Biolegend and are listed in **Supplemental Table 2**. Flow cytometric analysis was performed with FACSVerse (BD).

Single Cell Ca^{2+} Imaging

T cells were loaded in suspension with 1 μM Fura 2-AM in AIMV medium at room temperature for 20–25 min and seeded on poly-ornithine coated glass coverslips. All experiments were at room temperature as in (34). For stimulation of store operated Ca^{2+} influx 1 μM Thapsigargin (Tg) was used. Where indicated cells were treated 5 or 20 μM caloxin1 C2. Analyzed parameters include: maximum $[Ca^{2+}]_i$ (Peak), steady state $[Ca^{2+}]_i$ analyzed as the average $[Ca^{2+}]_i$ 25 s before removal of $[Ca^{2+}]_o$ (Plateau), and the fraction of retained $[Ca^{2+}]_i$ (Plateau/Peak) calculated for each cell independently. Analysis of the efflux rates was performed using Origin software. To test the influence of $[Ca^{2+}]_i$ on PMCA activity, cells were binned according to their peak or plateau $[Ca^{2+}]_i$ (iso-cells) to facilitate comparison of the corresponding efflux rates in the presence or absence of extracellular Ca^{2+}, respectively.

Transcription Factors Binding Site Analysis

A 5,000 bp long sequence upstream to start codon of *ATP2B4* was used as a potential promoter sequence for *ATP2B4*.

Prediction of transcription factor potentially regulating PMCA was done using the algorithms provided by three different data bases: ChIP-Seq (35), HOCOMOCO (36), and Promo V3 (37). Identification of transcription factor binding site (TFBS) was done by Emsembl Trancription Factor tool [Enembl Regulatory Build (38)], and making use of the matrix-based transcription factor binding site in JASPAR database (39). Results obtained from the independent data bases were subject to Venn analysis using the online tool Venny 2.1 (40) to detect common results, listed in **Supplementary Table 1**.

Chromatin Immunoprecipitation

To test binding of transcription factors to PMCA4b promoter region, antibodies against transcription factors (YY1 or NFAT, cell signaling, 3 µg each) or isotype control antibodies (rabbit IgG or mouse IgG, respectively) were coupled to protein A/G agarose beads (Santa Cruz) in coupling buffer (0.01 M sodium phosphate, 0.15 M NaCl, pH 7.2) overnight at 4°C then cross-linked to the beads using 5 mM BS3 (Thermoscientific). In parallel, human $CD4^+$ T cells were harvested, washed then cross-linked with PBS then containing 5 mM DSP (Thermoscientific) and 3% PFA for 20 min at 4°C. Excess cross-linker and PFA were quenched by 125 mM Glycine in PBS. Cell pellets were lysed in 20 mM Tris, 100 mM KCl, 10% glycerine (v/v), 0.5% n-Octyl-β-D-glucopyranoside (Merck Millipore). Finally lysates were subjected to chromatin shearing with Qsonica Sonicator Q700 (Thermoscientific) in total processing time of 4 min, 20 s laps of 40% amplitude and 10 s pauses. Clear lysates were diluted to 1 ml with binding buffer [20 mM Tris, 100 mM KCl, 10% glycerine (v/v)]. An aliquot of 50 µl was kept as an input control. Lysates were incubated with preclearing beads (isotype IgG bound beads) for 3 h at 4°C; unbound lysate was allowed to bind to control IgG (a fresh aliquot of isotype IgG bound beads) for 3 h at 4°C, and finally unbound lysate was bound to chromatin IP beads (transcription factor bound beads) for 3 h at 4°C. Beads collected at different steps were washed with standard low salt, high salt, LiCl buffer, and finally with TE according to Thermoscientific protocol. Finally, DNA was eluted with 1% SDS in 100 mM NaHCO3, purified using DNA purification kit (Qiagen), and used as template to test for binding of the PMCA4b promoter region using Q5 hot start polymerase (NEB biolabs) and the primers: forward 5′-CACCACCGTGCCAGCTAA-3′, reverse 3′-GAAGGGTGCTAGTTGGACA-5′. Amplicons were visualized by DNA agarose, and identity was confirmed by Sanger sequencing.

Dual Luciferase Reporter Assay

To estimate alterations in PMCA4 promoter activity, the region (Gene ID NG_029589.1, bp 663-1052) identified by ChIP assay to be potentially bound by YY1 was amplified with similar primers as above mentioned but adding SacI and NheI recognition sequences. The corresponding cDNA was subcloned into pGL3 basic (Promega, no. E1751) upstream to sequence encoding red firefly luciferase. Three days before conducting the assay, HEK293 cells were transfected with siRNA targeting YY1 (siYY1) (Accel Human YY1 siRNA SMART pool, no. E-011796-00-0010, Horizon) or with non-silencing control RNA (ns). Forty-eight hours later, cells were transfected with the created plasmid (PMCA Promoter, PP) or pGL3 basic (ϕ) together with plasmid encoding green renilla luciferase under thymidine kinase promoter control (pTK-Green Renilla Luciferase, ThermoFisher Scientific, no. 16154) in a DNA ratio of 2:1. Finally, 24 h later, cells were stimulated with 5 ng/ml phorbol 12-myristate 13-acetate (PMA) and 500 ng/ml ionomycin for 6 h then lysed in passive lysis buffer commercially provided in the dual luciferase reporter assay kit (Promega, no. E1910). Assay was conducted according to the manufacturer's instructions, and luminescence measurements were done using CLARIOstar (BMG, LABTEC) at gain of 3,600. For analysis, red firefly luciferase luminescence was normalized to the green renilla luciferase and data presented as average ± SEM of the relative change to the control condition of each independent experiment.

RNA Isolation, cDNA Synthesis, and Quantitative Real-Time PCR

The indicated cell types were harvested and stored at −80°C until RNA was isolated using RNeasy kit (Qiagen) following the manufacturer's instructions. SuperScriptTMII Reverse Transcriptase (Life technologies) was used to generate complementary DNA (cDNA), and subsequent qRT-PCR was conducted using QuantiTect SYBR Green Kit (Qiagen) and a CFX96 Real-Time System (Biorad). For quantification, threshold cycle (Cq) values of a gene of interest were normalized to that of either RNA polymerase or to TATA box binding protein (TBP) using the δCq method. For comparison of mRNA levels between two or more populations, fold change was calculated with $2^{-\Delta\Delta Cq}$ method.

Western Blot

For protein expression analysis, cells were harvested, washed with PBS then lysed in buffer containing 20 mM Tris, 100 mM KCl, 10% glycerine (v/v), 0.5% n-Dodecyl beta Maltoside (DDM), pH 7.4. Lysates were stored at −80° until analyzed. Standard SDS-PAGE was performed followed by electrotransfer to nitrocellulose membranes. Immunoblots were probed with anti-Orai1 (Sigma, catalogue number O8264), anti-STIM1 (Proteintech, # 11565-1-A), anti-STIM2 (Sigma, # S8572), anti-GAPDH (Cell Signaling, clone 14C10) anti-β-actin (Abcam, clone AC-15) or anti-PMCA4 (Thermoscientific, clone JA9) at a 1:1,000 dilution. For protein detection, an enhanced chemiluminescence detection reagent was used (Clarity Western ECL Substrate, Biorad). Densitometric quantification of detected protein bands was done with Quantity one software (Biorad).

Statistical Analysis

For analysis of Ca^{2+} imaging data, 100–250 cells were measured per experiment; one to two independent experiments were done per donor up to 14 donors. Otherwise, data is presented as mean ± S.E.M. Data was tested for normal distribution. When comparing two groups, statistical significance was tested by

performing unpaired, two-tailed Student t-test for normally distributed data sets and Mann–Whitney test when samples are not normally distributed or when the sample size was not sufficient to test for normality. Comparing more than two groups was done using Kruskal–Wallis one-way analysis of variance (ANOVA) or conventional ANOVA when data showed normal distribution and equal variance. Asterisks indicate significant differences for different p values as follows: * $p < 0.05$, ** $p < 0.01$, *** $p < 0.001$. Statistical analysis was performed using Graphpad Prism.

RESULTS

Differential Expression of PMCA4b Results in Distinct SOCE Profiles in CD4$^+$ Naïve and Memory Cells

In our previous work we characterized the SOCE profiles of antiCD3/CD28-activated cells, *in vitro* polarized into CD4$^+$ T cell subtypes (Th1, Th2, Th17, and Treg) and observed that the control naïve and memory cells that were activated but cultured in non-polarizing conditions showed differential SOCE profiles with concomitant upregulation of PMCA in the activated memory cells (34). Therefore, we set out in the current work to investigate whether in resting cells PMCA plays a differential role in Ca^{2+} homeostasis and thus regulates the differentiation process of human CD4$^+$ T cells. First, we measured SOCE profiles in resting naïve ($CD4^+CD127^{high}CD25^-CD45RO^-$) and memory ($CD4^+CD127^{high}CD25^-CD45RO^+$) CD4$^+$ T cells. We isolated the desired populations from human peripheral blood mononuclear cells (PBMCs) using the fluorescence activated cell sorting (FACSorting) strategy shown (**Figure S1**) where we excluded regulatory cells (Treg, $CD4^+CD127^{low}CD25^+$) and sorted the desired populations from conventional CD4$^+$ T cells ($CD4^+CD127^{high}CD25^-$). One day later, we measured changes of intracellular Ca^{2+} concentration following thapsigargine (Tg)-induced store depletion. The resulting SOCE profiles of naïve and memory human CD4$^+$ cells were significantly distinct. Naïve cells showed a higher peak and plateau of $[Ca^{2+}]_i$ than memory cells (**Figures 1A, B**). The observation that the peak $[Ca^{2+}]_i$ of memory cells was reduced by 13.5% while the steady state plateau $[Ca^{2+}]_i$ and the fraction of retained Ca^{2+} (Plateau/Peak) were reduced by more than 40% each compared to naïve cells indicates that Ca^{2+} signals in memory cells exhibit faster decay kinetics. To determine whether the difference in naïve and memory profiles is due to differential expression of Ca^{2+} influx and/or extrusion mechanisms, we analyzed the expression of the relevant genes. First, we analyzed the expression levels of *ORAI1–3* and *STIM1–2*, the main constituents of Ca^{2+} influx pathways in T cells. Analysis of mRNA (**Figure 1C**) and protein (**Figures 1D, E**) levels showed that both naïve and memory CD4$^+$ cells express comparable levels of SOCE components. The specificity of the antibodies was validated by cells where *ORAI1* (41), *STIM1*, or *STIM2* (42) was deleted by CRISPR-Cas9 mediated gene targeting. Using commercially available antibodies for ORAI2 and ORAI3 proteins we were unable to reliably detect endogenous proteins. These results indicate that reduced $[Ca^{2+}]_i$ is likely not explained by reduced Ca^{2+} influx through ORAI channels and imply involvement of Ca^{2+} efflux mechanisms. Analysis of expressed isoform of plasma membrane Ca^{2+} dependent ATPase (PMCA, *ATP2B1-4*) revealed that the main isoforms expressed in CD4$^+$ cells are PMCA1 (*ATP2B1*) and the more predominant PMCA4 (*ATP2B4*) in agreement with (12) while isoforms PMCA2 (*ATP2B2*) and PMCA3 (*ATP2B3*) were not detected (**Figure 1F**). Furthermore, using splice-specific primers, mRNA analysis showed that PMCA4b (*ATP2B4b*) is the main variant in CD4$^+$ T cells (**Figure 1G**). Interestingly, memory cells showed a significantly higher expression level of PMCA4b (*ATP2B4b*) on both mRNA level (**Figure 1H**) and protein (**Figures 1I, J**) level, using an antibody with tested specificity [(43) and **Figures S2A, B**]. Moreover, we analyzed Ca^{2+} efflux rates in the presence (**Figure 1K**) and after removal (**Figure 1L**) of extracellular Ca^{2+}, taking into consideration the Ca^{2+} dependence of PMCA activity (1, 2). Binning the cells according to $[Ca^{2+}]_i$ allowed comparison of cells with similar $[Ca^{2+}]_i$ (iso-cells) and revealed that memory cells extrude Ca^{2+} with higher rates (**Figures 1K, L**) and shorter time constants (τ) (**Figures S2C, D**) compared to naïve cells independent of the cytosolic $[Ca^{2+}]$. Significant differences are observed at physiologically relevant concentrations but not at higher concentrations probably due to exceeding pumping capacity of PMCA but also due to the small fraction of cells exhibiting this concentration, which hampers statistical significance.

Pharmacological Inhibition or Downregulation of PMCA Reverses SOCE Phenotypes of Memory Cells

To directly test whether PMCA has a differential role in Ca^{2+} homeostasis in resting CD4$^+$ T cell subsets, we tested the effect of pharmacological inhibition of PMCA by caloxin1C2 (C1C2) (44) on SOCE profiles of naïve and memory cells. Treatment with 5 μM or 20 μM caloxin1C2 only mildly altered SOCE profile of the naïve cells resulting in no or a slight increase that did not exceed 14% of the tested parameters (**Figures 2A, B**). On the other hand, memory cells treated acutely with the PMCA blocker showed a significantly increased SOCE resulting in a 58% increase of the plateau and 47% increase of the fraction of retained Ca^{2+} compared to untreated cells (**Figures 2C, D**). Noteworthy is that the application of 20 μM, a concentration shown to block all PMCA isoforms (44), did not result in additional effects on the plateau levels compared to the application of the PMCA4-specific inhibitory concentration of 5 μM (**Figures 2C, D** compare blue to gray traces and dots) indicating that PMCA4 is indeed the main functional isoform in T cells and in agreement with the expression analyses (**Figures 1F–J**).

In a second approach we transfected naïve or memory CD4$^+$ T cells using an *ATP2B4* specific siRNA (siPMCA) that resulted in significant downregulation on RNA (**Figure S2A**) and protein levels (**Figure S2B**). Similar to the pharmacological manipulation by C1C2, downregulation of PMCA4 led to no or subtle alteration of analyzed parameters of SOCE profile of the naïve cells (**Figures 3A, B**). Memory cells treated with siPMCA

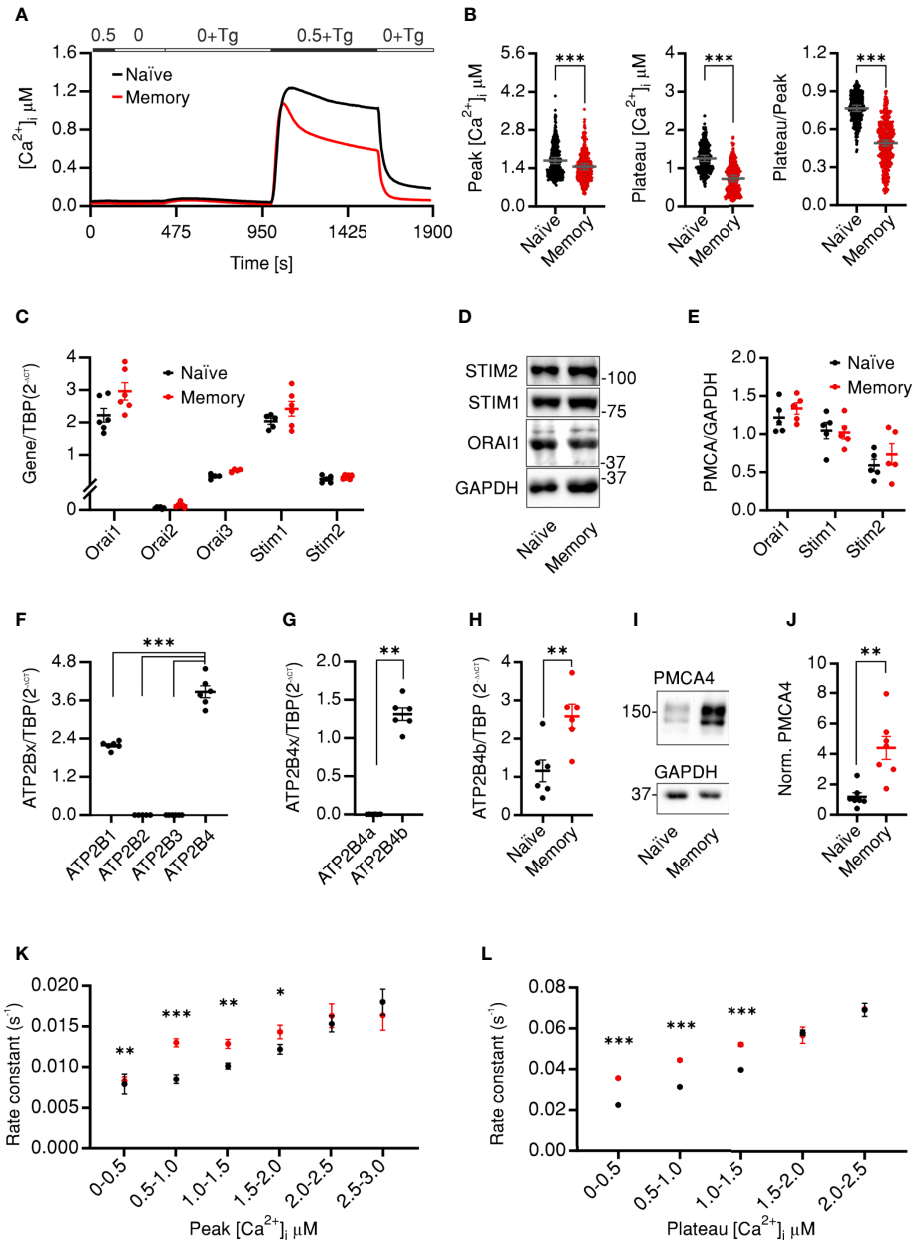

FIGURE 1 | CD4 naïve and memory cells have distinct SOCE profiles due to differential expression of PMCA4b **(A)** Average traces showing changes of $[Ca^{2+}]_i$ over time in response to changes of extracellular solutions containing the shown $[Ca^{2+}]_o$ indicated in the bar above the traces. SOCE was measured in human naïve ($CD4^+CD127^{high}CD25^-CD45RO^-$, black) or memory ($CD4^+CD127^{high}CD25^-CD45RO^+$, red) cells isolated from PBMCs. **(B)** Bar graphs showing analyzed parameters of SOCE measured in **(A)**. **(C)** The relative expression of *ORAI1–3* and *STIM1–2* mRNA in cells measured **(A)**. **(D)** Representative of five independent Western blots (WB) and corresponding quantification **(E)** analyzing the expression of ORAI1, STIM1, and STIM2 in cells measured in **(A)**. **(F–H)** Quantitative RT-PCR analysis showing **(F)** the relative expression of the four isoforms of PMCA **(G)** relative expression of the splice variants 4a and 4b in total $CD4^+$ cells, and **(H)** relative expression of PMCA4b in naïve (black) and memory (red) cells isolated as in **(A)** from human PBMCs. **(I)** Representative of five independent WB and corresponding quantification **(J)** showing the expression of PMCA4 in cells measured in **(A, H)**. **(K)** Analysis of Ca^{2+} efflux rates (see *Materials and Methods*) in the presence of $[Ca^{2+}]_o$ in iso-cells measured in **(A)** as a function of peak $[Ca^{2+}]_i$. **(L)** Analysis of Ca^{2+} efflux rates after removal of $[Ca^{2+}]_o$ in cells measured in **(A)** as a function of plateau $[Ca^{2+}]_i$. Data represent average ± s.e.m. obtained from 3,257 and 2,644 cells measured in 22 and 23 independent experiments (shown dots in **A, B**), five to six independent experiments **(C–J)**. Asterisks indicate significance at ** $p < 0.01$, *** $p < 0.001$ using unpaired two-tailed Student t-test **(B)**, Mann–Whitney test **(G, J)** or Kruskal–Wallis one-way analysis of variance (ANOVA) **(C–F)**.

showed a 15% increased influx peak, while the plateau was increased by 49% compared to memory cells transfected with non-silencing RNA (ns) resulting in significant increase in fraction of Ca^{2+} retained in the cells (Plateau/Peak ratio) (**Figures 3C, D**). These results indicate a differential role of PMCA in Ca^{2+} homeostasis of naïve and memory cells.

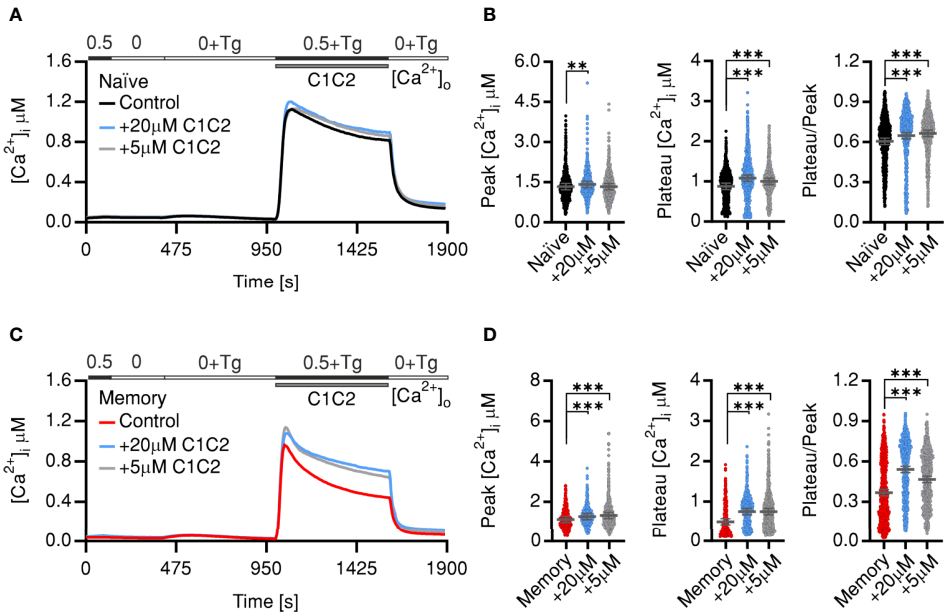

FIGURE 2 | Pharmacological inhibition of PMCA reverts SOCE phenotypes of memory cells. Average traces showing changes of $[Ca^{2+}]_i$ over time in response to changes of extracellular solutions containing the shown $[Ca^{2+}]_o$ indicated in the bar above the traces. SOCE was measured in human naïve (**A**, black) or memory (**C**, red) control cells or corresponding cells treated with 20 μM Caloxin1C2 (blue), or with 5 μM Caloxin1C2 (gray). **(B, D)** Bar graphs showing analyzed parameters of SOCE measured in **(A, C)**, respectively. Data represent average ± s.e.m obtained from 976 to 2,659 cells, measured in 8–10 independent experiments. Asterisks indicate significance at $^{**}p < 0.01$, $^{***}p < 0.001$ using Kruskal–Wallis one-way analysis of variance (ANOVA).

In Vivo Developed Effector and Memory CD4⁺ Cellular Compartments Differentially Express PMCA4 and Exhibit Corresponding SOCE Profiles

The findings presented so far compared the Ca^{2+} signals and expression profiles of naïve and memory cells. Memory cells ($CD4^+CD45RO^+$), however, represent a heterologous population that is commonly divided into different compartments depending on effector and proliferative capacities of the cells. Therefore, our next aim was to answer the question whether *in vivo* developed memory compartments show distinct PMCA expression profiles or do they homogenously share higher expression levels of PMCA. To address this question, we FACSorted $CD4^+$ T cell compartments from human PBMCs based on the surface markers (CD45RO/CCR7) as illustrated in (**Figure 4A**). Purity of the sorted populations was tested by post-sorting staining (**Figure 4B**). Cells that were $CCR7^+CD45RO^-$ $CD45RA^+$ are defined as naïve cells (N), $CCR7^+CD45RO^+$ CD $45RA^-$ as central memory cells (CMs), $CCR7^-CD45RO^+$ $CD45RA^-$ as effector memory (EM) and $CCR7^-CD45RO^-$ CD $45RA^+$ as terminally differentiated effector memory cells (EMRA) (45–47). T_{EMRA} cells are a poorly characterized population of T cells expressing CD45RA but are commonly used due to the sharing functional properties with the short lived effector cells (15, 48, 49). For further characterization, we measured the expression of IFNγ which showed the expected pattern where the EMRA and EM populations had higher expression of IFNγ than the CM while it was lacking in naïve cells (**Figure 4C**).

Interestingly, analysis of PMCA expression in the sorted populations revealed differential expression profiles: with the terminally differentiated effector (EMRA) and EM cells showing the higher expression than CM and naïve cells (**Figure 4D**). Finally, we tested whether SOCE profiles of the *in vivo* differentiated cellular compartments recapitulate the differentially expressed PMCA levels. Indeed, measurements of Tg-induced Ca^{2+} influx showed that $CD4^+$ compartments have distinct SOCE profiles with comparable Ca^{2+} peaks (**Figures 4E, F**) but distinct increase in decay rates resulting in the lowest plateau $[Ca^{2+}]_i$ and retained Ca^{2+} fractions for the effector cells (EMRA and EM), intermediate levels for CM cells while the naïve cells have the highest plateau $[Ca^{2+}]_i$ and retained Ca^{2+} fractions (**Figures 4E, F**) in line with the observed PMCA expression levels (**Figure 4D**). These differences are underlined by parallel differences in the efflux rates in presence of (**Figure S3A**) and after removal (**Figure S3B**) of extracellular Ca^{2+} indicating that the differences in the plateau and retained Ca^{2+} fractions are indeed due to differential expression and function of PMCA.

PMCA4 Regulates Compartment Stoichiometry Upon Activation

The outcome of an immune response depends on the dynamics of mobilization of T cells within naïve and memory

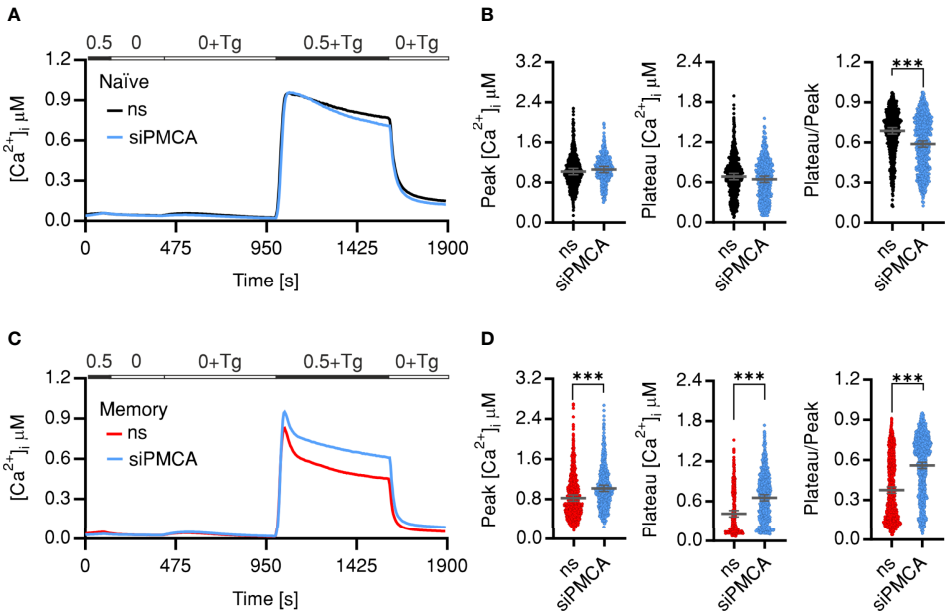

FIGURE 3 | Downregulation of PMCA reverts SOCE phenotypes of memory cells. Average traces showing changes of $[Ca^{2+}]_i$ over time in response to changes of extracellular solutions as shown in the bar above the traces. SOCE was measured in human naïve (**A**, ns, black) or memory (**C**, ns, red) cells transfected with non-silencing RNA or transfected with PMCA4 targeting siRNA (siPMCA, blue). **(B, D)** Bar graphs showing analyzed parameters of SOCE measured in **(A, C)**. Data represent average ± s.e.m obtained from 1,163 to 1,280 cells, measured in 7–10 independent experiments (shown dots). Asterisks indicate significance at, ***$p < 0.001$ using Kruskal–Wallis one-way analysis of variance (ANOVA).

compartments. Furthermore, our findings show that $CD4^+$ cellular compartments exhibit differential SOCE profiles and PMCA expression levels. Therefore, we sought to address if and how regulation of $[Ca^{2+}]_i$ by PMCA4 contributes to fate-decision making concerning compartment distribution of $CD4^+$ T cells upon activation. To this end, we isolated naïve $CD4^+$ T cells from PBMCs to exclude effects of previous antigen exposure and on the following day transfected naïve cells with non-silencing RNA (ns) or with siRNA targeting *ATP2B4* (siPMCA). Three days later, naïve cells were replenished with fresh siRNA, subjected to stimulation using antiCD3/CD28 coated beads, and monitored for compartment distribution 24 h later. The experimental design and the surface markers used to assign activated cells into different compartments are shown in **Figure 5A**. Downregulation of *ATP2B4* did not alter stoichiometry of cellular compartments as defined by CD45RO or CD45RA and CCR7 (**Figures S3C, D**). Because, classically, T cell compartments are defined based on CD45RO, CD45RA, CCR7, and CD62L (45–47), and CD62L is commonly used as an alternative marker for CCR7 for compartment definition (50, 51), we analyzed compartment stoichiometry based on CD45RO and CD62L expression. Interestingly, this analysis showed that downregulation of *ATP2B4* resulted in a significant decrease of the fraction of cells in terminally differentiated effector memory $CD45RA^+$ compartment T_{EMRA} ($CD4^+CD62^-LCD45RO^-$), while the fraction of cells remaining in the naïve compartment ($CD4^+CD62L^+CD45RO^-$) was significantly increased compared to cells treated with non-silencing RNA (**Figures 5B, C**). The effects on EM and CM compartments showed similar tendencies as the effects observed on EMRA and naïve compartments, respectively, albeit not significant (**Figures 5B, C**).

To test whether downregulation of PMCA4 is accompanied by altered potential of naïve $CD4^+$ cells to be activated, we measured the expression level of activation markers CD69 and CD154 under the same experimental conditions as above. Despite the reduced fraction of effector cells, treatment of naïve cells with siPMCA resulted in increased expression of activation marker CD154 (CD40L) (**Figures 5D, E**), while expression of CD25 was not altered (**Figure S3E**). These results imply that PMCA4 downregulation does not inhibit activation *per se* but rather regulates the compartment stoichiometry.

Transcriptional Control of PMCA Results in Biphasic Expression Following Activation

The experiments described above provide evidence that PMCA4 expression level correlates with the cellular compartment of $CD4^+$ T cells and contributes to regulation of compartment stoichiometry. To explore potential underlying mechanisms, we set out to investigate transcriptional regulation of PMCA expression. To this end, we explored potential transcription factor binding sites (TFBSs) in the promoter region of PMCA (*ATP2B4*) using available ChIP seq information (35) combined with TFBS prediction data bases HOCOMOCO (36) and Promo 3 (37, 52). The resulting analyses (**Figure 6A**) predicted 33 transcription factors (listed in **Supplementary Table 1**) that were detected in all three algorithms with the transcription

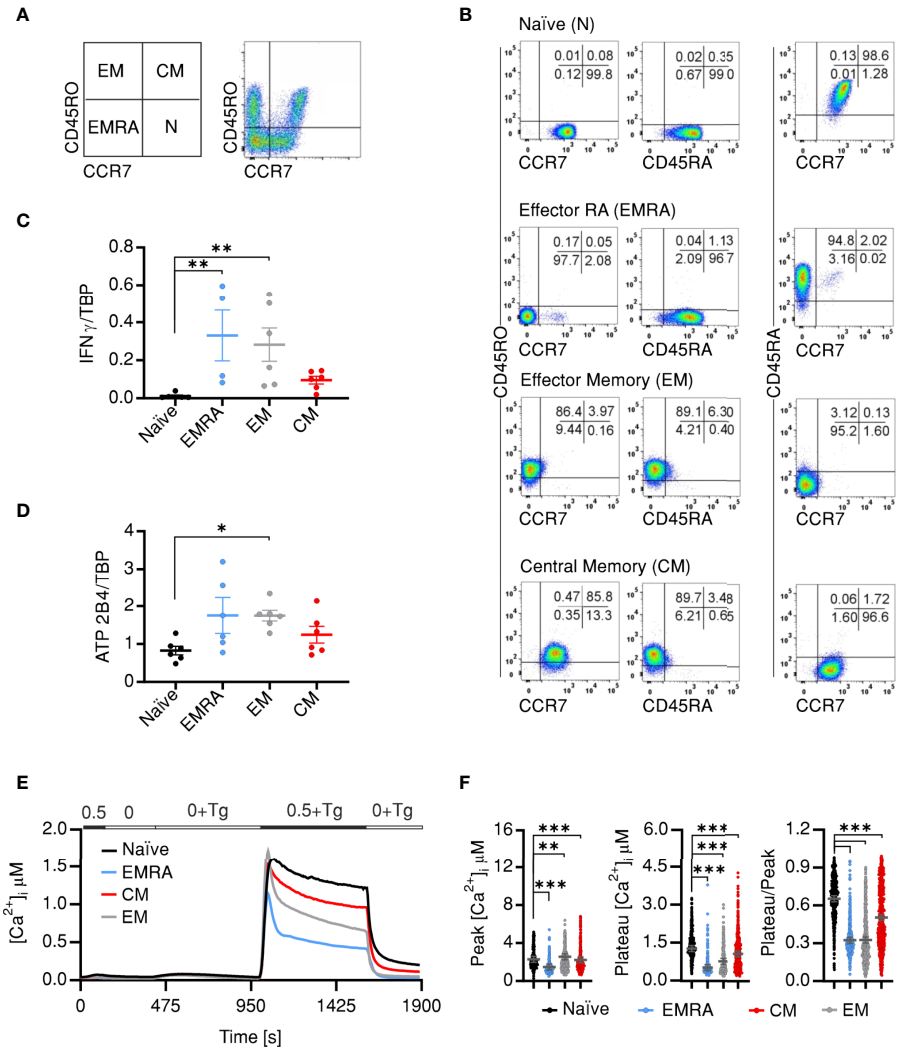

FIGURE 4 | In vivo CD4$^+$ effector and memory compartments differentially express PMCA and exhibit corresponding SOCE profiles **(A)** Representative images showing sorting strategy of CD4$^+$ cells into the different compartments using the shown surface markers and according to the shown scheme. **(B)** Representative images obtained by post-sorting flow cytometric analysis of the sorted cells. Quantitative RT-PCR analysis showing relative expression of *IFNG* **(C)** and PMCA4 (*ATP2B4*) **(D)** relative to TBP, in CD4$^+$ compartments isolated as in **(A)**. **(E)** Average traces showing changes of $[Ca^{2+}]_i$ over time in response to changes of extracellular solutions as shown in the bar above the traces, analyzed in CD4$^+$ T cell compartments isolated as in **(A)**. **(F)** Bar graphs showing analyzed parameters of SOCE measured in **(E)**. Data represent average ± s.e.m obtained from 586 to 1,084 cells measured in six independent experiments. Asterisks indicate significance at *p < 0.05, **p < 0.01 and ***p < 0.001 using Kruska–Wallis one-way analysis of variance (ANOVA).

factor YY1 having the highest predicted score. Consequently, we explored whether we can experimentally confirm binding of YY1 to the promoter region of PMCA. Because our preliminary experiments showed that a conventional protocol of chromatin immune precipitation (ChIP) experiments was prone to misleading positive results, we applied a rigorous protocol that eliminates all unspecific binding using isotype control antibody bound beads in a "pre-clearing" step (**Figure 6B** first lane). The efficiency of elimination of unspecific binding was demonstrated by applying the pre-cleared lysate to fresh isotype control antibody-bound beads (**Figure 6B** second lane). Finally, the ability of YY1 to bind to the promoter region was tested by using a YY1-specific antibody to immunoprecipitate YY1 and the bound genomic DNA which was then amplified with specific primers, designed based on the predicted binding domains. In parallel, we used an anti-NFAT antibody to serve as an additional control for the specificity of binding. Results of the ChIP experiments showed that YY1, but not NFAT, was able to bind the promoter region of PMCA4 as visualized on agarose gels (**Figure 6B**). The identity of the amplicon was further confirmed by sequencing.

To investigate whether the levels of YY1 are altered in CD4$^+$ cell compartments similar to PMCA, we analyzed expression levels in naïve and memory CD4$^+$ cells. Surprisingly, the

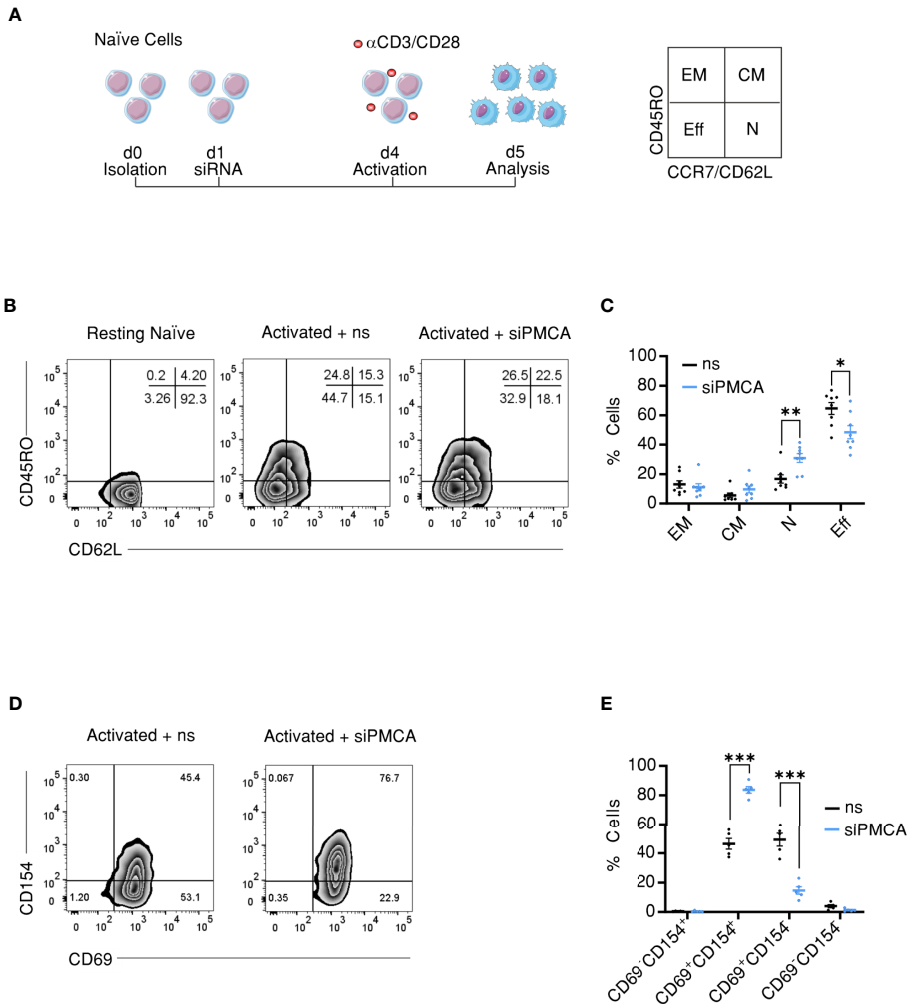

FIGURE 5 | Downregulation of PMCA alters compartment stoichiometry upon activation of naïve CD4$^+$ T cells. **(A)** Schematic representation of the experimental design: naïve cells were isolated from human PBMCs using FACSorting, transfected one day later with control non silencing RNA (ns) or with siRNA targeting PMCA4 (siPMCA), stimulated with antiCD3/CD28 coated beads 72 h following transfection and 24 h later analyzed for compartment distribution using flow cytometry and the shown surface markers. **(B)** Representative flow cytometric analysis images showing compartment distribution in resting naïve cells (left image) or naïve cells transfected with control non-silencing RNA (ns, middle image) or transfected with siRNA targeting PMCA4b (siPMCA, right image) then activated following time scheme shown in **(A)**. **(C)** Frequency of cells (% Cells) measured in the EM (CD62L$^-$CD45RO$^+$), CM (CD62L$^+$CD45RO$^+$), N (CD62L$^+$CD45RO$^-$) and EMRA (CD62L$^-$CD45RO$^-$) compartments following treatment with non-silencing RNA (ns, black) or siRNA targeting PMCA4 (siPMCA, blue) according to time scheme shown in **(A)**. **(D)** Representative flow cytometric analysis images showing expression of the activation markers CD154 and CD69 in cells treated as in **(A, B)**. **(E)** Frequency of cells (% Cells) measured in **(D)** and expressing activation markers following treatment with non-silencing RNA (ns, black) or siRNA targeting PMCA4b (siPMCA, blue) according to time scheme shown in **(A)**. Data represent average ± s.e.m obtained from eight independent experiments. Asterisks indicate significance at *$p < 0.05$, **$p < 0.01$ using Kruskal–Wallis one-way analysis of variance (ANOVA).

expression level of YY1 was comparable to the resting naïve and memory CD4$^+$ cells (**Figures 6C, D**). We hypothesized that this finding might be due to performing the analysis in resting cells where YY1 expression is adapted to steady state levels. To test this hypothesis, we stimulated total CD4$^+$ cells for 24 h using antiCD3/CD28 coated beads, and indeed we observed an increased level of YY1 concomitant to decreased expression of PMCA (**Figures 6E, F**), indicating that YY1 represses PMCA levels upon stimulation, resulting in reduced Ca^{2+} clearance compared to unstimulated cells (**Figures S4A, B**). Because PMCA levels were decreased after acute stimulation (**Figures 6E, F**) contrary to the increased levels we observed in resting memory compared to naïve cells (**Figures 1H–J**), we extended the expression analysis to examine whether YY1 alters PMCA4 expression in association with long term stimulation and full differentiation of T cells. To this end, we subjected the naïve cells to *in vitro* polarization protocol providing stimulatory, co-stimulatory, and cytokine mediated signals necessary for differentiation of naïve cells into Th1 or Treg cells (34). This experiment not only aims to monitor changes of PMCA and YY1

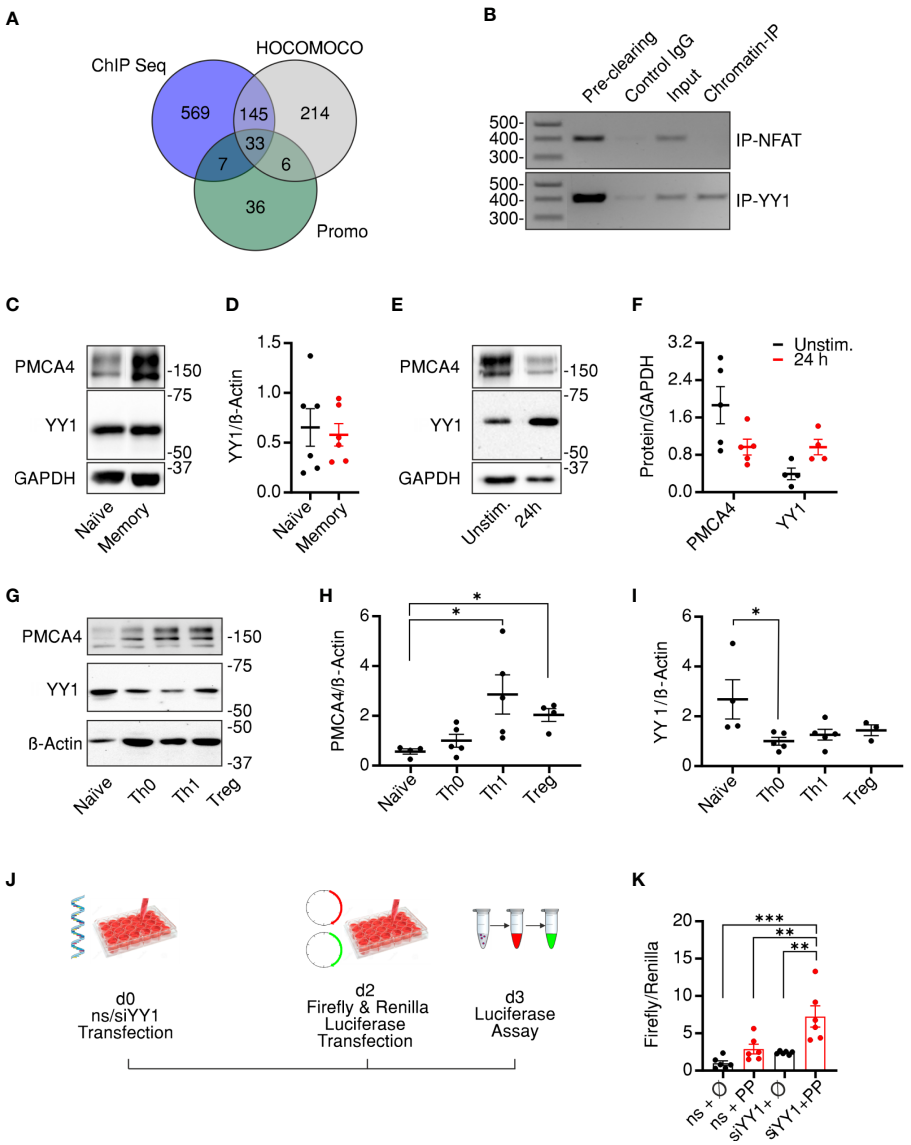

FIGURE 6 | Transcriptional control of PMCA results in biphasic expression following activation. **(A)** Venn diagram showing the overlapping results obtained from three data bases (HOCOMOCO, Promo V3 and Chip-seq) used to predict transcriptional factors binding to PMCA4 promoter region (see also *Materials and Methods* and *Supplementary Materials*). **(B)** Agarose gel showing PCR amplicons obtained by using primers designed to amplify a 410 base pair-long fragment of the PMCA4b (*ATP2B4b*) promoter region. Poly chain reactions (PCRs) were performed using chromatin DNA purified from total lysate (Input) or after immune precipitation by pre-clearing beads, beads bound to IgG control antibodies, beads bound to anti-NFAT (upper row, Chromatin-IP) or to anti-YY1 (lower row, Chromatin-IP). **(C)** Representative of five WBs and corresponding quantification **(D)** showing analysis of PMCA4 and YY1 in resting naïve or memory $CD4^+$ T cells isolated as in **Figure 1**. **(E)** Representative of five WBs and corresponding quantification **(F)** showing analysis of PMCA4 and YY1 in total $CD4^+$ T cells in resting conditions (Unstim.) or after 24 h stimulation with antiCD3/CD28 coated beads (24 h). **(G)** Representative of five WBs and corresponding quantification **(H, I)** showing analysis of PMCA4 **(H)** and YY1 **(I)** in naïve $CD4^+$ T cells before (Naïve) and after 7 d culture in control (Th0) or polarizing conditions into Th1 or regulatory (Treg) cells. **(J)** Schematic representation of experimental design of promoter assay: HEK293 cells were transfected with non-silencing RNA (ns) or with siRNA targeting YY1 (siYY1). On day 2, cells were transfected with plasmids expressing red firefly or green renilla luciferases and the dual luciferase assay was conducted on day 3. **(K)** Firefly luminescence normalized to Renilla luminescence in cells transfected as in **(J)** with firefly luciferase expressed in plasmid without promoter (ϕ) or with PMCA promoter (PP). Asterisks indicate significance at *$p < 0.05$, **$p < 0.01$ or ***$p < 0.001$ using Kruskal–Wallis one-way analysis of variance (ANOVA).

expression levels upon longer stimulation but also monitors correlation of PMCA expression to developing effector functions. The polarized cells showed the expected differential expression of *IFNG* (**Figure S4C**) and *FOXP3* (**Figure S4D**), the hallmarks of Th1 and Treg populations, respectively. Importantly, terminally differentiated effector cells (Th1, Treg) showed a significant upregulation of PMCA4, while the control cells which were stimulated in non-polarizing conditions (Th0)

underwent milder upregulation of PMCA (**Figures 6G, H** and **Figure S4E**). Strikingly, levels of YY1 followed a reverse pattern: while YY1 underwent transient upregulation within 24 h of activation (**Figures 6E, F**) YY1 expression decreased upon longer activation (**Figures 6G, I** and **Figure S4F**), in line with the equal levels analyzed in resting cells (**Figures 6C, D**).

Finally, we aimed to confirm that altered expression of PMCA is due to direct regulation by YY1. To achieve this correlation, we constructed a plasmid expressing red firefly luciferase under transcriptional control of the identified PMCA promoter region where YY1 is predicted to bind (**Figures 6A, B**). To facilitate analysis of promoter activity independent of transfection efficiency, the red firefly luciferase activity was normalized to the co-transfected green renilla luciferase expressed under the transcriptional control of TK promoter. To address whether the PMCA promoter activity is directly regulated by YY1, we downregulated YY1 using siRNA (**Figures S4G, H**) then conducted the dual luciferase assay (**Figures 6J**). Measurements (**Figure 6K**) show that in cells transfected with non-silencing RNA (ns), the PMCA promoter (ns + PP) was able to induced expression of the firefly luciferase compared to control cells (ns + ϕ). More importantly, the PMCA promoter activity is significantly increased following downregulation of YY1 (siYY1 + PP). Collectively, these results point towards YY1 being part of the transcriptional factor complex regulating PMCA promoter activity to allow T cells to adapt the expression of PMCA4 to fulfill cellular requirements of Ca^{2+} during different phases of an immune response.

DISCUSSION

In the current work we investigated how Ca^{2+} signals are fine-tuned during activation of $CD4^+$ T cells to regulate the stoichiometry of $CD4^+$ T cell compartments and thus the outcome of an immune response. Using fura-2 Ca^{2+} imaging we show that quiescent memory cells accommodate a lower $[Ca^{2+}]_i$ and are able to clear the Ca^{2+} signals faster than their naïve counter parts (**Figures 1A, B**). Comparable levels of expressed SOCE genes (**Figures 1C–E**) but significantly more expressed PMCA4b (**Figures 1F–J**) and higher efflux rates independent of $[Ca^{2+}]_i$ (**Figures 1K, L** and **Figures S2C, D**) present strong evidence that SOCE phenotype of memory cells is mostly a result of more efficient clearance machinery. Furthermore, analysis of the contribution of PMCA to Ca^{2+} homoeostasis in naïve and memory cells by applying an acute pharmacological inhibition approach (**Figure 2**) as well as by directly downregulating *ATP2B4* (PMCA4) (**Figure 3**) presents evidence that clearly supports the hypothesis that PMCA4 plays a functionally more significant role in Ca^{2+} clearance in memory compared to naïve $CD4^+$ T cells. Further analysis of the $CD4^+$ T cell subpopulations revealed that the quiescent cells in the naïve and central memory compartments express less PMCA and exhibit slower Ca^{2+} signal decay kinetics than compartments associated with more effector functions (EMRA and EM) (**Figure 4**). *In vitro* generation of effector populations (Th1, Treg) able to express effector hallmarks (**Figures S4C, D**) and the concomitant significant increase in PMCA (**Figures 6G, H**) strongly support the hypothesis that fully differentiated effector cells acquire higher expression of PMCA to guard against apoptosis resulting from activation induced $[Ca^{2+}]_i$ overloads. Noteworthy is that, before cells reach full differentiation state, PMCA levels transiently decrease after short term stimulation (**Figures 6E, F**) allowing $[Ca^{2+}]_i$ levels required to fulfill cellular demands during initial proliferation.

$CD4^+$ T cell differentiation is a complex process in which a plethora of genes are rigorously orchestrated, and we hypothesized that PMCA4 is an important regulator of this process. To gain a direct insight into the regulatory role of PMCA4 in $CD4^+$ T cell differentiation, we monitored differentiation and compartment distribution upon activation of naïve cells while downregulating PMCA4 (siPMCA). We found that siPMCA-treated cells exhibit a skewed compartment stoichiometry following activation with more cells remaining in the naïve compartment parallel to a decreased fraction of cells able to reach the effector compartments (EM and EMRA) (**Figures 5B, C**). Interestingly, although CD62L and CCR7 are often co-expressed and are commonly considered equivalent for population definition (46, 50), we observed an effect of PMCA4 downregulation on the expression of CD62L (**Figures 5B, C**) but not of CCR7 (**Figure S3C**). This might be explained by the different kinetics of expression of both molecules where activated T cells rapidly shed CD62L of their surface and gain new set of selectins which allow them to migrate to non-lymphoid tissues (53). Moreover, a $CD62L^-CCR7^+$ population has been identified as a frequently existing memory population (54) and was detected in cancer studies where it has been shown to have homing and effector functions that are distinct from conventional CM and EM, though much less understood (55). These results implicate an importance of PMCA4 in regulating early events of activation.

Our analysis of the effect of downregulation of PMCA on activation markers revealed differential effects. Transcriptional upregulation of the activation marker CD69 is triggered immediately (30–60 min) upon activation and reaches measurable levels already after 2–3 h (56) then declines within 6 h (57). These fast kinetics could indicate that CD69 is regulated by mechanisms independent of PMCA and $[Ca^{2+}]_i$ and thus explain our finding that total frequency of cells expressing CD69 was not altered by siPMCA treatment (**Figures 4D, E**). On the other hand, downregulation of PMCA4 resulted in a significant increase of fraction of cells expressing CD154 (CD40L). CD154 belongs to the TNF gene family, and its upregulation follows a biphasic pattern with the first phase being TCR dependent and taking place within the first 24 h after activation. The later phase is dependent on the cytokine composition in the cellular milieu (58, 59). Furthermore, CD154 transcription is enhanced by Ca^{2+} -NFAT pathway (60, 61) which together with an increased NFAT activity upon downregulation of PMCA4 (62) might explain the increase observed in CD154 expression in siPMCA-treated cells (**Figures 4D, E**). Together, these findings

support our hypothesis that PMCA is essential for regulating differentiation processes in functional $CD4^+$ T cells.

By virtue of their ability to activate, repress, or modify gene expression, transcription factors regulate cell division, differentiation, and function (63). Transcriptional control of PMCA isoforms has been addressed (64, 65) but remains to time, however, poorly understood. Here we applied *in silico* analyses (**Figure 6A**) and identified YY1, a ubiquitously expressed transcription factor (66), to be likely involved in the modulation of PMCA4 expression. Indeed, we confirmed that YY1 binds specifically to a predicted sequence in the PMCA4 promoter region (**Figure 6B**). Furthermore, our results suggest a repressive effect of YY1 on PMCA expression, as indicated by the inverse correlation between expression of PMCA4 and that of YY1 over the course of differentiation (**Figures 6E–I**) and more importantly, by the increased PMCA promoter activity upon downregulation of YY1 (**Figures 6J, K**). There are several lines of evidence for the interaction between YY1 and c-myc (67–69). c-Myc inhibits the DNA binding capacity of YY1 (69) in a direct, binding-independent (67) but c-Myc concentration dependent manner (69). Moreover, Habib and co-workers have shown that in B-cells c-Myc regulates differentiation and function by mechanisms including downregulation of PMCA (64). Therefore, we hypothesize that PMCA4 is regulated by a complex of transcription factors including c-Myc and YY1 (Zeller et al., 2006, Habib et al., 2007). If and how individual members of this complex have reciprocal effects needs further investigation. By regulating PMCA4 levels and thereby shaping Ca^{2+} signals, the activities of calcineurin and NFAT, and thus T cell differentiation are modulated. With an upregulation approach, the importance of PMCA to clear near plasma membrane Ca^{2+} thus allowing for NFAT activation was also demonstrated (70). Our results suggest a scenario in which another layer of transcriptional control regulates T cell differentiation and activity in which upstream to the PMCA-Calcineurn/NFAT line, expression of PMCA is regulated by YY1/c-Myc. Furthermore, it is plausible to speculate that the net outcome of transcriptional regulation depends on the expression of the individual components of such a transcription factor complex which makes it difficult to establish direct causal relationships in studies addressing a single transcription factor.

Together, our data suggest a model in which PMCA4 plays a pivotal role in shaping Ca^{2+} signals in different activation states of $CD4^+$ T cells. This role is under a biphasic transcriptional regulation by YY1. The first phase starts once $CD4^+$ T cells are activated where YY1 is upregulated and represses PMCA expression so that $CD4^+$ T cells can accommodate higher cytosolic $[Ca^{2+}]_i$ levels to support gene expression and proliferation. In the second phase, the initial repression by YY1 is alleviated, and PMCA expression increases to guard against $[Ca^{2+}]_i$ overloads and promote survival of effector cells and formation of long lasting memory cells that are able to efficiently mediate faster immune response upon subsequent antigen encounter.

DATA AVAILABILITY STATEMENT

The datasets presented in this study can be found in online repositories. The names of the repository/repositories and accession number(s) can be found in the article/**Supplementary Material**.

ETHICS STATEMENT

Blood samples were collected from healthy donors in the Institute of Clinical Hemostaseology and Transfusion Medicine, Saarland University, Homburg. Research was approved by the local ethical committee (83/15; FOR2289-TP6, Niemeyer/Alansary), and blood donors provided their written consent. The patients/participants provided their written informed consent to participate in this study.

AUTHOR CONTRIBUTIONS

All authors conceptualized the study and edited the manuscript. MM-W and DA performed the experiments and data analysis. BN and DA secured funding and resources. DA wrote the manuscript. All authors contributed to the article and approved the submitted version.

FUNDING

This work is supported by the Deutsche Forschungsgemeinschaft DFG (FOR 2289-P6) to BN and DA and (TRR219-C09) to BN. The FACSverse was funded by DFG (GZ: INST 256/423-1 FUGG).

ACKNOWLEDGMENTS

We kindly thank Dr. Eichler and the Institute for Clinical Hemostaseology and Transfusion Medicine for providing donor blood, Dr. Schwarz for supervising primary cell isolation and critical reading of MS, Dr. Hoth for technical and equipment support and critical reading of MS, Anja Bergsträßer and Dr. Krause from the FACS Facility of the Institute of Physiology (DFG grant 207087572) for help with cell sorting, Carmen Hässig, and Kathrin Förderer for technical assistance and Dr. Martin Hart and Tim Kehl for help with the TFBS analysis, and Dr. Prates-Roma and Dr. Frisch for help with promoter assays.

SUPPLEMENTARY MATERIAL

The Supplementary Material for this article can be found online at: https://www.frontiersin.org/articles/10.3389/fimmu.2021.687242/full#supplementary-material

Supplementary Figure 1 | Sorting strategy of naïve and memory cells Representative flow cytometry images showing the isolation FACSorting strategy of human naïve ($CD4^+CD127^{high}CD25^-CD45RO^-$) or memory ($CD4^+CD127^{high}CD25^-CD45RO^+$) T cells using FACSAria III (BD).

Supplementary Figure 2 | siRNA-mediated downregulation of PMCA and analysis of time constants of Ca^{2+} efflux rates of naïve and memory cells **(A)** Quantitative RT-PCR analysis showing relative expression level of PMCA4 in naïve (black) and memory (red) cells transfected with non-silencing RNA (ns) or with siRNA targeting PMCA4 (siPMCA). **(B)** Representative WB showing PMCA4 expression in total CD4 T cells transfected with non-silencing RNA (ns) or with siRNA targeting PMCA4 (siPMCA). **(C)** Analysis of time constants (Tau) of Ca^{2+} efflux rates in presence of $[Ca^{2+}]o$ in cells measured in Figure 1A as function of peak $[Ca^{2+}]i$ **(D)** Analysis of time constants (Tau) of Ca2+ efflux rates after removal of [Ca2+]0 in cells measured in in **Figure 1A** as function of plateau $[Ca^{2+}]i$.

Supplementary Figure 3 | Ca2+efflux rates in CD4 compartments and effects of downregulation of PMCA on surface markers. **(A)** Analysis of Ca^{2+} efflux rates in presence of $[Ca^{2+}]o$ in cells measured in **Figure 4E** as function of peak [Ca2+]i **(B)** Analysis of Ca^{2+} efflux rates after removal of $[Ca^{2+}]o$ in cells measured in in **Figure 4F** as function of plateau $[Ca^{2+}]i$. **(C–E)** Average fractions of cells expressing the indicated surface markers as obtained by flow cytometry analysis of naïve cells transfected with non-silencing RNA (ns, black) or with siRNA targeting PMCA4 (siPMCA, blue) for 72 h then stimulated with antiCD3/CD28 coated beads for further 24 h as in **Figure 5**.

Supplementary Figure 4 | SOCE profile and expression analysis of genes of interest in activated cells **(A)** Average traces showing changes of [Ca**2+**]i over time in response to changes of extracellular solutions containing the shown [Ca**2+**]o indicated in the bar above the traces. SOCE was measured in resting total human $CD4^+$ cells (Unstim., black) or following a 24h antiCD3/CD28 coated bead stimulation (24h, red). **(B)** Bar graphs showing analyzed parameters of SOCE measured in **(A). (C–E)** Quantitative RT-PCR analysis of IFNG **(C)**, FOXP3 **(D)**, ATP2B4 **(E)** or YY1 **(F)** measured in resting naive $CD4^+$ T cells (naïve) or cells cultured for 7 d under control conditions (Th0) or conditions to polarize cells into Th1 or Treg. **(G)** Quantitative RT-PCR analysis showing relative expression level of YY1 in total CD4+ T cells transfected with non-silencing RNA (ns) or with siRNA targeting YY1 (siYY1). **(B)** Representative WB showing YY1 expression in total $CD4^+$ T cells transfected with non-silencing RNA (ns) or with siRNA targeting YY1 (siYY1).

REFERENCES

1. Bautista DM, Hoth M, Lewis RS. Enhancement of Calcium Signalling Dynamics and Stability by Delayed Modulation of the Plasma-Membrane Calcium-ATPase in Human T Cells. *J Physiol* (2002) 541:877–94. doi: 10.1113/jphysiol.2001.016154
2. Bautista DM, Lewis RS. Modulation of Plasma Membrane Calcium-ATPase Activity by Local Calcium Microdomains Near CRAC Channels in Human T Cells. *J Physiol* (2004) 556:805–17. doi: 10.1113/jphysiol.2003.060004
3. Lewis RS. Calcium Signaling Mechanisms in T Lymphocytes. *Annu Rev Immunol* (2001) 19:497–521. doi: 10.1146/annurev.immunol.19.1.497
4. Samakai E, Hooper R, Martin KA, Shmurak M, Zhang Y, Kappes DJ, et al. Novel STIM1-dependent Control of Ca2+ Clearance Regulates NFAT Activity During T-cell Activation. *FASEB J* (2016) 30:3878–86. doi: 10.1096/fj.201600532R
5. Kiang JG, McClain DE, Warke VG, Krishnan S, Tsokos GC. Constitutive NO Synthase Regulates the Na+/Ca2+ Exchanger in Human T Cells: Role of [Ca2+]i and Tyrosine Phosphorylation. *J Cell Biochem* (2003) 89:1030–43. doi: 10.1002/jcb.10564
6. Launay S, Bobe R, Lacabaratz-Porret C, Bredoux R, Kovacs T, Enouf J, et al. Modulation of Endoplasmic Reticulum Calcium Pump Expression During T Lymphocyte Activation. *J Biol Chem* (1997) 272:10746–50. doi: 10.1074/jbc.272.16.10746
7. Stafford N, Wilson C, Oceandy D, Neyses L, Cartwright EJ. The Plasma Membrane Calcium Atpases and Their Role as Major New Players in Human Disease. *Physiol Rev* (2017) 97:1089–125. doi: 10.1152/physrev.00028.2016
8. Supper V, Schiller HB, Paster W, Forster F, Boulegue C, Mitulovic G, et al. Association of CD147 and Calcium Exporter PMCA4 Uncouples IL-2 Expression From Early Tcr Signaling. *J Immunol* (2016) 196:1387–99. doi: 10.4049/jimmunol.1501889
9. Brini M, Cali T, Ottolini D, Carafoli E. The Plasma Membrane Calcium Pump in Health and Disease. *FEBS J* (2013) 280:5385–97. doi: 10.1111/febs.12193
10. Gong D, Chi X, Ren K, Huang G, Zhou G, Yan N, et al. Structure of the Human Plasma Membrane Ca(2+)-ATPase 1 in Complex With its Obligatory Subunit Neuroplastin. *Nat Commun* (2018) 9:3623. doi: 10.1038/s41467-018-06075-7
11. Strehler EE, Zacharias DA. Role of Alternative Splicing in Generating Isoform Diversity Among Plasma Membrane Calcium Pumps. *Physiol Rev* (2001) 81:21–50. doi: 10.1152/physrev.2001.81.1.21
12. Caride AJ, Filoteo AG, Penheiter AR, Paszty K, Enyedi A, Penniston JT. Delayed Activation of the Plasma Membrane Calcium Pump by a Sudden Increase in Ca2+: Fast Pumps Reside in Fast Cells. *Cell Ca* (2001) 30:49–57. doi: 10.1054/ceca.2001.0212
13. Korthals M, Langnaese K, Smalla KH, Kahne T, Herrera-Molina R, Handschuh J, et al. A Complex of Neuroplastin and Plasma Membrane Ca (2+) Atpase Controls T Cell Activation. *Sci Rep* (2017) 7:8358. doi: 10.1038/s41598-017-08519-4
14. Schmidt N, Kollewe A, Constantin CE, Henrich S, Ritzau-Jost A, Bildl W, et al. Neuroplastin and Basigin are Essential Auxiliary Subunits of Plasma Membrane Ca(2+)-ATPases and Key Regulators of Ca(2+) Clearance. *Neuron* (2017) 96:827–38.e829. doi: 10.1016/j.neuron.2017.09.038
15. Durek P, Nordstrom K, Gasparoni G, Salhab A, Kressler C, de Almeida M, et al. Epigenomic Profiling of Human Cd4(+) T Cells Supports a Linear Differentiation Model and Highlights Molecular Regulators of Memory Development. *Immunity* (2016) 45:1148–61. doi: 10.1016/j.immuni.2016.10.022
16. Farber DL, Yudanin NA, Restifo NP. Human Memory T Cells: Generation, Compartmentalization and Homeostasis. *Nat Rev Immunol* (2014) 14:24–35. doi: 10.1038/nri3567
17. Sallusto F, Lanzavecchia A. Heterogeneity of CD4+ Memory T Cells: Functional Modules for Tailored Immunity. *Eur J Immunol* (2009) 39:2076–82. doi: 10.1002/eji.200939722
18. Ahmed R, Bevan MJ, Reiner SL, Fearon DT. The Precursors of Memory: Models and Controversies. *Nat Rev Immunol* (2009) 9:662–8. doi: 10.1038/nri2619
19. Christie D, Zhu J. Transcriptional Regulatory Networks for CD4 T Cell Differentiation. *Curr Top Microbiol Immunol* (2014) 381:125–72. doi: 10.1007/82_2014_372
20. Schoettler N, Hrusch CL, Blaine KM, Sperling AI, Ober C. Transcriptional Programming and T Cell Receptor Repertoires Distinguish Human Lung and Lymph Node Memory T Cells. *Commun Biol* (2019) 2:411. doi: 10.1038/s42003-019-0657-2
21. Jain J, McCaffrey PG, Miner Z, Kerppola TK, Lambert JN, Verdine GL, et al. The T-cell Transcription Factor NFATp is a Substrate for Calcineurin and Interacts With Fos and Jun. *Nature* (1993) 365:352–5. doi: 10.1038/365352a0
22. Rao A, Luo C, Hogan PG. Transcription Factors of the NFAT Family: Regulation and Function. *Annu Rev Immunol* (1997) 15:707–47. doi: 10.1146/annurev.immunol.15.1.707
23. Mayer SI, Thiel G. Calcium Influx Into MIN6 Insulinoma Cells Induces Expression of Egr-1 Involving Extracellular Signal-Regulated Protein Kinase and the Transcription Factors Elk-1 and CREB. *Eur J Cell Biol* (2009) 88:19–33. doi: 10.1016/j.ejcb.2008.07.002
24. Savignac M, Mellstrom B, Naranjo JR. Calcium-Dependent Transcription of Cytokine Genes in T Lymphocytes. *Pflugers Arch* (2007) 454:523–33. doi: 10.1007/s00424-007-0238-y
25. Vig M, Peinelt C, Beck A, Koomoa DL, Rabah D, Koblan-Huberson M, et al. CRACM1 is a Plasma Membrane Protein Essential for Store-Operated Ca2+ Entry. *Science* (2006) 312:1220–3. doi: 10.1126/science.1127883
26. Zhang SL, Yeromin AV, Zhang XH, Yu Y, Safrina O, Penna A, et al. Genome-Wide RNAi Screen of Ca(2+) Influx Identifies Genes That Regulate Ca(2+)

Release-Activated Ca(2+) Channel Activity. *Proc Natl Acad Sci USA* (2006) 103:9357–62. doi: 10.1073/pnas.0603161103
27. Liou J, Kim ML, Heo WD, Jones JT, Myers JW, Ferrell JEJr., et al. STIM is a Ca2+ Sensor Essential for Ca2+-store-depletion-triggered Ca2+ Influx. *Curr Biol* (2005) 15:1235–41. doi: 10.1016/j.cub.2005.05.055
28. Roos J, DiGregorio PJ, Yeromin AV, Ohlsen K, Lioudyno M, Zhang S, et al. STIM1, an Essential and Conserved Component of Store-Operated Ca2+ Channel Function. *J Cell Biol* (2005) 169:435–45. doi: 10.1083/jcb.200502019
29. Zhang SL, Yu Y, Roos J, Kozak JA, Deerinck TJ, Ellisman MH, et al. STIM1 is a Ca2+ Sensor That Activates CRAC Channels and Migrates From the Ca2+ Store to the Plasma Membrane. *Nature* (2005) 437:902–5. doi: 10.1038/nature04147
30. Ritchie MF, Yue C, Zhou Y, Houghton PJ, Soboloff J. Wilms Tumor Suppressor 1 (WT1) and Early Growth Response 1 (EGR1) are Regulators of STIM1 Expression. *J Biol Chem* (2010) 285:10591–6. doi: 10.1074/jbc.M109.083493
31. Ritchie MF, Zhou Y, Soboloff J. Transcriptional Mechanisms Regulating Ca(2+) Homeostasis. *Cell Ca* (2011) 49:314–21. doi: 10.1016/j.ceca.2010.10.001
32. Knorck A, Marx S, Friedmann KS, Zophel S, Lieblang L, Hassig C, et al. Quantity, Quality, and Functionality of Peripheral Blood Cells Derived From Residual Blood of Different Apheresis Kits. *Transfusion* (2018) 58:1516–26. doi: 10.1111/trf.14616
33. Neron S, Thibault L, Dussault N, Cote G, Ducas E, Pineault N, et al. Characterization of Mononuclear Cells Remaining in the Leukoreduction System Chambers of Apheresis Instruments After Routine Platelet Collection: A New Source of Viable Human Blood Cells. *Transfusion* (2007) 47:1042–9. doi: 10.1111/j.1537-2995.2007.01233.x
34. Kircher S, Merino-Wong M, Niemeyer BA, Alansary D. Profiling Calcium Signals of In Vitro Polarized Human Effector CD4(+) T Cells. *Biochim Biophys Acta* (2018) 1865:932–43. doi: 10.1016/j.bbamcr.2018.04.001
35. Ambrosini G, Dreos R, Kumar S, Bucher P. The ChIP-Seq Tools and Web Server: A Resource for Analyzing ChIP-seq and Other Types of Genomic Data. *BMC Genomics* (2016) 17:938. doi: 10.1186/s12864-016-3288-8
36. Kulakovskiy IV, Vorontsov IE, Yevshin IS, Sharipov RN, Fedorova AD, Rumynskiy EI, et al. HOCOMOCO: Towards a Complete Collection of Transcription Factor Binding Models for Human and Mouse Via Large-Scale ChIP-Seq Analysis. *Nucleic Acids Res* (2018) 46:D252–9. doi: 10.1093/nar/gkx1106
37. Messeguer X, Escudero R, Farre D, Nunez O, Martinez J, Alba MM. PROMO: Detection of Known Transcription Regulatory Elements Using Species-Tailored Searches. *Bioinformatics* (2002) 18:333–4. doi: 10.1093/bioinformatics/18.2.333
38. Zerbino DR, Wilder SP, Johnson N, Juettemann T, Flicek PR. The Ensembl Regulatory Build. *Genome Biol* (2015) 16:56. doi: 10.1186/s13059-015-0621-5
39. Fornes O, Castro-Mondragon JA, Khan A, van der Lee R, Zhang X, Richmond PA, et al. JASPAR 2020: Update of the Open-Access Database of Transcription Factor Binding Profiles. *Nucleic Acids Res* (2020) 48:D87–92. doi: 10.1093/nar/gkz1001
40. Oliveros JC. Venny. An Interactive Tool for Comparing Lists With Venn's Diagrams (2007). Available at: https://bioinfogp.cnb.csic.es/tools/venny/index.html.
41. Alansary D, Peckys DB, Niemeyer BA, de Jonge N. Detecting Single ORAI1 Proteins Within the Plasma Membrane Reveals Higher-Order Channel Complexes. *J Cell Sci* (2020) 133(1):jcs240358. doi: 10.1242/jcs.240358
42. Ramesh G, Jarzembowski L, Schwarz Y, Konrad M, Poth V, Schwaer G, et al. Short Novel STIM1B Uncovers a Mechanism of Synaptic Enhancement. *Cell Rep* (2021) 34(11):108844–54. doi: 10.2139/ssrn.3707638
43. Ho PW, Pang SY, Li M, Tse ZH, Kung MH, Sham PC, et al. PMCA4 (ATP2B4) Mutation in Familial Spastic Paraplegia Causes Delay in Intracellular Calcium Extrusion. *Brain Behav* (2015) 5:e00321. doi: 10.1002/brb3.321
44. Pande J, Szewczyk MM, Grover AK. Allosteric Inhibitors of Plasma Membrane Ca Pumps: Invention and Applications of Caloxins. *World J Biol Chem* (2011) 2:39–47. doi: 10.4331/wjbc.v2.i3.39
45. Mahnke YD, Brodie TM, Sallusto F, Roederer M, Lugli E. The Who's Who of T-cell Differentiation: Human Memory T-cell Subsets. *Eur J Immunol* (2013) 43:2797–809. doi: 10.1002/eji.201343751
46. Sallusto F, Lenig D, Forster R, Lipp M, Lanzavecchia A. Two Subsets of Memory T Lymphocytes With Distinct Homing Potentials and Effector Functions. *Nature* (1999) 401:708–12. doi: 10.1038/44385
47. Tian Y, Babor M, Lane J, Schulten V, Patil VS, Seumois G, et al. Unique Phenotypes and Clonal Expansions of Human CD4 Effector Memory T Cells Re-Expressing CD45RA. *Nat Commun* (2017) 8:1473. doi: 10.1038/s41467-017-01728-5
48. Henson SM, Riddell NE, Akbar AN. Properties of End-Stage Human T Cells Defined by CD45RA Re-Expression. *Curr Opin Immunol* (2012) 24:476–81. doi: 10.1016/j.coi.2012.04.001
49. Sallusto F, Geginat J, Lanzavecchia A. Central Memory and Effector Memory T Cell Subsets: Function, Generation, and Maintenance. *Annu Rev Immunol* (2004) 22:745–63. doi: 10.1146/annurev.immunol.22.012703.104702
50. Eichmann M, Baptista R, Ellis RJ, Heck S, Peakman M, Beam CA. Costimulation Blockade Disrupts Cd4(+) T Cell Memory Pathways and Uncouples Their Link to Decline in Beta-Cell Function in Type 1 Diabetes. *J Immunol* (2020) 204:3129–38. doi: 10.4049/jimmunol.1901439
51. Priesner C, Aleksandrova K, Esser R, Mockel-Tenbrinck N, Leise J, Drechsel K, et al. Automated Enrichment, Transduction, and Expansion of Clinical-Scale Cd62l(+) T Cells for Manufacturing of Gene Therapy Medicinal Products. *Hum Gene Ther* (2016) 27:860–9. doi: 10.1089/hum.2016.091
52. Farre D, Roset R, Huerta M, Adsuara JE, Rosello L, Alba MM, et al. Identification of Patterns in Biological Sequences at the ALGGEN Server: PROMO and MALGEN. *Nucleic Acids Res* (2003) 31:3651–3. doi: 10.1093/nar/gkg605
53. Bajnok A, Ivanova M, Rigo JJr., Toldi G. The Distribution of Activation Markers and Selectins on Peripheral T Lymphocytes in Preeclampsia. *Mediators Inflammation* (2017) 2017:8045161. doi: 10.1155/2017/8045161
54. Unsoeld H, Pircher H. Complex Memory T-cell Phenotypes Revealed by Coexpression of CD62L and CCR7. *J Virol* (2005) 79:4510–3. doi: 10.1128/JVI.79.7.4510-4513.2005
55. Xie YL, BW, Yuan XD, Tian PK, Ou X, et al. Expression Characteristics of Surface Markers of Memory T Cells, CD45RO, CCR7 and CD62L, in Tumor-infiltrating Lymphocytes in Liver Cancer Tissues of Patients With Hepatocellular Carcinomas. *J Clin Cell Immunol* (2013) 4(6). doi: 10.4172/2155-9899.1000181
56. Reddy M, Eirikis E, Davis C, Davis HM, Prabhakar U. Comparative Analysis of Lymphocyte Activation Marker Expression and Cytokine Secretion Profile in Stimulated Human Peripheral Blood Mononuclear Cell Cultures: An In Vitro Model to Monitor Cellular Immune Function. *J Immunol Methods* (2004) 293:127–42. doi: 10.1016/j.jim.2004.07.006
57. Cibrian D, Sanchez-Madrid F. CD69: From Activation Marker to Metabolic Gatekeeper. *Eur J Immunol* (2017) 47:946–53. doi: 10.1002/eji.201646837
58. Lee BO, Haynes L, Eaton SM, Swain SL, Randall TD. The Biological Outcome of CD40 Signaling is Dependent on the Duration of CD40 Ligand Expression: Reciprocal Regulation by Interleukin (IL)-4 and IL-12. *J Exp Med* (2002) 196:693–704. doi: 10.1084/jem.20020845
59. Roy M, Waldschmidt T, Aruffo A, Ledbetter JA, Noelle RJ. The Regulation of the Expression of gp39, the CD40 Ligand, on Normal and Cloned CD4+ T Cells. *J Immunol* (1993) 151:2497–510.
60. Daoussis D, Andonopoulos AP, Liossis SN. Targeting CD40L: A Promising Therapeutic Approach. *Clin Diagn Lab Immunol* (2004) 11:635–41. doi: 10.1128/CDLI.11.4.635-641.2004
61. Wu SF, Chang CB, Hsu JM, Lu MC, Lai NS, Li C, et al. Hydroxychloroquine Inhibits CD154 Expression in CD4(+) T Lymphocytes of Systemic Lupus Erythematosus Through NFAT, But Not STAT5, Signaling. *Arthritis Res Ther* (2017) 19:183. doi: 10.1186/s13075-017-1393-y
62. Boczek T, Lisek M, Ferenc B, Zylinska L. Cross Talk Among PMCA, Calcineurin and NFAT Transcription Factors in Control of Calmodulin Gene Expression in Differentiating PC12 Cells. *Biochim Biophys Acta Gene Regul Mech* (2017) 1860:502–15. doi: 10.1016/j.bbagrm.2017.01.012
63. Shi Y, Lee JS, Galvin KM. Everything You Have Ever Wanted to Know About Yin Yang 1. *Biochim Biophys Acta* (1997) 1332:F49–66. doi: 10.1016/S0304-419X(96)00044-3
64. Habib T, Park H, Tsang M, de Alboran IM, Nicks A, Wilson L, et al. Myc Stimulates B Lymphocyte Differentiation and Amplifies Calcium Signaling. *J Cell Biol* (2007) 179:717–31. doi: 10.1083/jcb.200704173
65. Ximenes HM, Kamagate A, Van Eylen F, Carpinelli A, Herchuelz A. Opposite Effects of Glucose on Plasma Membrane Ca2+-ATPase and Na/Ca Exchanger

Transcription, Expression, and Activity in Rat Pancreatic Beta-Cells. *J Biol Chem* (2003) 278:22956–63. doi: 10.1074/jbc.M212339200
66. Gordon S, Akopyan G, Garban H, Bonavida B. Transcription Factor YY1: Structure, Function, and Therapeutic Implications in Cancer Biology. *Oncogene* (2006) 25:1125–42. doi: 10.1038/sj.onc.1209080
67. Austen M, Cerni C, Luscher-Firzlaff JM, Luscher B. YY1 can Inhibit c-Myc Function Through a Mechanism Requiring DNA Binding of YY1 But Neither its Transactivation Domain Nor Direct Interaction With C-Myc. *Oncogene* (1998) 17:511–20. doi: 10.1038/sj.onc.1201968
68. Riggs KJ, Saleque S, Wong KK, Merrell KT, Lee JS, Shi Y, et al. Yin-Yang 1 Activates the C-Myc Promoter. *Mol Cell Biol* (1993) 13:7487–95. doi: 10.1128/MCB.13.12.7487
69. Shrivastava A, Yu J, Artandi S, Calame K. YY1 and c-Myc Associate In Vivo in a Manner That Depends on c-Myc Levels. *Proc Natl Acad Sci USA* (1996) 93:10638–41. doi: 10.1073/pnas.93.20.10638
70. Go CK, Hooper R, Aronson MR, Schultz B, Cangoz T, Nemani N, et al. The Ca(2+) Export Pump PMCA Clears Near-Membrane Ca(2+) to Facilitate Store-Operated Ca(2+) Entry and NFAT Activation. *Sci Signal* (2019) 12 (602):eaaw2627. doi: 10.1126/scisignal.aaw2627

Conflict of Interest: The authors declare that the research was conducted in the absence of any commercial or financial relationships that could be construed as a potential conflict of interest.